THERMAL ENERGY STORAGE AND DYNAMIC THERMAL MANAGEMENT OF 5G BASE STATIONS BASED ON GRAPHENE COMPOSITE PHASE CHANGE MATERIALS

by

Shuai YANG *

Hebi Polytechnic, Hebi, Henan, China

Original scientific paper
https://doi.org/10.2298/TSCI2506257Y

This paper investigates the performance of composite PCM with varying graphene contents in 5G base station heat dissipation. Experiments and simulations demonstrate that 5.5% graphene forms 10-20 μm agglomerates (SEM confirmed), disrupting thermal networks. The 2.5% creates uniform 3-D paths, boosting conductivity to 2.3 W/mK without reducing latent heat, explaining superior cooling. In terms of temperature uniformity, the maximum temperature difference of the base station measured in the experiment is 11.1 ℃, and the simulation is 10.5 ℃, both of which are better than the 18.3 ℃ of pure paraffin. In the dynamic load cycle experiment, the temperature overshoot and recovery time of the experiment and simulation are close when the load changes suddenly, reflecting the good dynamic adjustment ability of the AHFAA algorithm.

Key words: *graphene composite PCM, thermal management, 5G base station, adaptive heat flow distribution algorithm, thermal energy storage*

Introduction

With the rapid popularisation of 5G communication technology, the global deployment of 5G base stations has grown exponentially. By 2024, China is expected to have built more than four million base stations, with over 100000 added every month. Due to the use of new technologies, such as large-scale antenna arrays, the power consumption of core components in 5G base stations is 3-5 times higher than that of 4G base stations. The average power consumption of a single station is 3000-5000 W, and the local heat flux density ranges from 80-120 W/cm². Actual measurements show that for every 10 ℃ increase in chip operating temperature, the equipment failure rate increases by 25%, the bit error rate increases by 15%, and the life span is shortened by more than 30%. Heat dissipation has become a key bottleneck restricting its stable operation [1]. The current mainstream thermal management solutions have limitations: due to the low thermal conductivity of air, the efficiency of air-cooled systems drops by more than 40% when the power density exceeds 50 W/cm², and the fan vibration noise interferes with the signal. The thermal conductivity of liquid cooling systems is better than that of air, but auxiliary equipment is required, energy consumption increases by 20%, maintenance costs increase by 30%, and outdoor deployment has the risk of freezing and leakage. Both are passive heat dissipation, which makes it challenging to match the instantaneous demand of the base station's dynamic load (10 times the flow difference between daytime and nighttime). During the summer, when temperatures are high, 15% of base stations shut down due

* Author's e-mail: hbzyyshuai@163.com

to overheating. The PCM can passively store heat and buffer temperature fluctuations, thereby maintaining a stable temperature. Paraffin has attracted attention due to its advantages, such as phase change temperature adaptation (40-60 °C). However, pure paraffin has low thermal conductivity and a delayed thermal response [2]. Graphene has high thermal conductivity, and composite PCM (GCPCM) made by mixing it with paraffin can build a 3-D thermal network to improve efficiency. This study aims to solve the dynamic thermal environment of 5G base stations, propose a thermal management system based on GCPCM, develop an adaptive heat flow distribution algorithm, study the material phase change dynamics and heat transfer mechanism, and optimize the doping ratio and packaging structure, aiming to break through the bottleneck of traditional technology and provide a high efficiency and low consumption solution [3].

Analysis of the characteristics of graphene composite phase change materials

Basics of phase change materials

The PCM can be categorised into three types based on their composition: organic, inorganic, and composite. Organic PCM, such as paraffin, achieve solid-liquid phase change through molecular lattice reconstruction [4]. The phase change process is non-corrosive and has a small volume change. Inorganic PCM, such as crystalline hydrated salts, rely on crystal structure dissociation undergo phase change. They have high latent heat but are prone to supercooling. Both use latent heat exchange during phase change to achieve temperature control [5]. The phase change temperature of paraffin is 25-60 °C, the latent heat is 200-250 kJ/kg, and the thermal conductivity is 0.2-0.3W/K. Paraffin chosen for 40-60 °C phase change (matching 5G operating temps) and 200-250 kJ/kg latent heat (10% higher than fatty acids). The phase change temperature of fatty acids is 30-55 °C, the latent heat is 180-220 kJ/kg, and the thermal conductivity is 0.18-0.25 W/K, but they are easily oxidized. The phase change temperature of hydrated salts is 50-85 °C, the latent heat is 220-300 kJ/kg, and the thermal conductivity is 0.5-0.8 W/mK, but there is a phase separation problem. The operating temperature of the core components of 5G base stations needs to be controlled at 40-65 °C. Paraffin is the preferred material due to its phase change range matching and good chemical stability. Its low thermal conductivity can be improved through composite modification. At the same time, the supercooling and phase separation problems associated with inorganic materials make it challenging to meet the long-term operational requirements of base stations [6].

Graphene characteristics and modification mechanism of phase change materials

Graphene is a 2-D honeycomb structure composed of a single layer of carbon atoms. The sp^2 hybridisation gives it an extremely high thermal conductivity (1000-5000 W/mK) and a specific surface area of 2630 m^2/g, which can build an efficient heat conduction path. Graphene forms a continuous heat conduction network within the PCM, and phonon-s are quickly transmitted along the carbon-carbon bonds, thereby reducing the interfacial thermal resistance. The 2.5% GCPCM achieves 2.3 W/mK (8× pure paraffin), measured via hot-wire method, ensuring it meets 5G thermal demands. Its surface functional groups interact with the matrix molecules to promote the transmission of thermal vibrations, significantly improving the overall thermal conductivity. An appropriate amount of graphene can reduce the volume expansion rate of PCM by 10%-15% and enhance the cycle stability, however, when the doping amount exceeds 5%, the latent heat will be reduced by 5%-8% due to agglomeration, and surface modification is required to balance the thermal conductivity and heat storage performance.

Construction of the 5G base station thermal management algorithm model

Establishment of 5G base station heat transfer model

Analysis and modelling of internal heat sources of base stations

The internal heat sources of 5G base stations are distributed in multiple dimensions. The core components and their respective heat generation proportions are power amplifier (PA, 45%), baseband processing unit (BBU, 25%), power supply module (PSU, 20%), and radio frequency module (RRU, 10%). The peak power of PA at full load is 800 W, and the junction temperature needs to be <85 °C. The BBU generates 300 W of heat, and the temperature threshold is 70 °C. The PSU generates 200 W of heat, and the RRU single module generates 50-80 W. Infrared thermal imaging shows that the heat source has a gradient distribution of *dense in the centre and sparse at the edge*. The heat flux density in the core area of PA and BBU is 60-80 W/cm², and drops to 10-20 W/20 W/cm² in the periphery [7]. The Gaussian distribution function can be used to construct a spatial model of the heat source intensity:

$$Q_{\mathrm{PA}}(x,y,z) = Q_{\mathrm{PA0}} \exp\left[-\frac{(x-x_0)^2+(y-y_0)^2}{2\sigma^2}\right]\delta(z-z_0) \tag{1}$$

where Q_{PAO} = 800 W is the rated heat generation power, (x_0, y_0, z_0) is the co-ordinate of the physical centre of PA, σ = 0.15 m calibrated via IR imaging, matching PA 50 mm hot zone radius. This ensures accurate heat distribution modelling. The diffusion coefficient of the BBU heat source model in the horizontal direction is increased to σ = 0.2 m to reflect its planar heat dissipation characteristics.

Mathematical description of the heat transfer process

The internal heat transfer of the base station is the result of the coupling of conduction, convection and radiation. The 3-D non-steady-state heat balance equation is:

$$\rho c_p \frac{\partial T}{\partial t} = \nabla(k\nabla T) + hA(T_a - T) + \epsilon\sigma_B A\left(T_s^4 - T^4\right) + Q_{\mathrm{total}} \tag{2}$$

where ρ [kgm^{-3}] is the material density, c_p [Jkg^{-1}K^{-1}] – the specific heat capacity at constant pressure, k [Wm^{-1}K^{-1}] – the thermal conductivity, h [Wm^{-2}K^{-1}] – the convective heat transfer coefficient, A [m^2] – the heat transfer area T_a [K] – the ambient temperature, ϵ – the surface emissivity, σ_B [5.67·10^{-8} Wm^{-2}K^{-4}] – the Boltzmann constant, T_s [K] – the temperature of the surrounding object, and Q_{total} [W] – the total heat source intensity.

For the area filled with GCPCM, the influence of phase change latent heat on energy balance needs to be considered, and the modified equation is:

$$\rho c_p \frac{\partial T}{\partial t} + \rho L \frac{\partial f}{\partial t} = \nabla(k\nabla T) + Q_{\mathrm{local}} \tag{3}$$

where L [Jkg^{-1}] is the latent heat of phase change, f – the liquid phase fraction ($0 \le f \le 1$), and the linear interpolation model $f = (T - T_{\mathrm{sol}})/(T_{\mathrm{liq}} - T_{\mathrm{sol}})$ used to describe the phase change process, T_{sol} and T_{liq} – the solid phase temperature and liquid phase temperature, respectively, and Q_{local} – the local heat source intensity, which is obtained by superimposing the heat source models of each component.

Design of adaptive heat flow allocation algorithm

The adaptive heat flow allocation algorithm (AHFAA) is based on the *perception-decision-execution* closed-loop control architecture. The core is to achieve precise heat flow control by dynamically adjusting the thermal resistance distribution of the GCPCM module. The base station is divided into six temperature control units (corresponding to three heat source areas and three heat dissipation channels), and each unit is equipped with an independent temperature sensor and a controllable thermal conductivity module. The algorithm introduces the heat flow sensitivity coefficient, λ_i, which is defined as the ratio of the unit temperature change rate to the heat flux density:

$$\lambda_i = \frac{\partial T_i / \partial t}{\partial q_i / \partial t} \tag{4}$$

where $\partial T/\partial t$ is the temperature change rate of the i temperature control unit and $\partial q_i/\partial t$ – the heat flux density change rate of the i temperature control unit. When λ_i exceeds the threshold, λ_{th}, it is determined that there is a risk of heat accumulation in the area, and it is necessary to accelerate heat dissipation by increasing heat flux distribution. The weight coefficient, w_i, is the core parameter of heat flux distribution, which satisfies the normalization condition $\sum_{i=1}^{6} w_i = 1$, and its dynamic adjustment is based on the coupling relationship between temperature deviation and heat flux sensitivity. A distributed fiber grating sensor array (spatial resolution 5 cm) is used to collect the temperature, $T_i(t)$, of each unit with a sampling frequency of 1 Hz. The ambient temperature, T_a, and heat source power, $Q(t)$, are recorded synchronously to construct a 3-D temperature field database. The temperature deviation is calculated:

$$\Delta T_i = T_i - T_{set} \tag{5}$$

where T_i is the actual temperature of the i temperature control unit and T_{set} = 55 °C – the target control temperature. The heat flux sensitivity is:

$$\lambda_i(t) = \frac{\dfrac{T_i(t) - T_i(t-1)}{\Delta t}}{\dfrac{q_i(t) - q_i(t-1)}{\Delta t}} \tag{6}$$

where $T_i(t)$ and $T_i(t-1)$ are the temperatures of the i temperature control unit at time t, and time $t-1$, respectively, $q_i(t)$ and $q_i(t)$ – the heat flux densities of the ith temperature control unit at time t and time $t-1$, and Δt is the sampling time interval. When $\Delta T_i > 0$, the update formula is executed:

$$w_i(t+1) = w_i(t) + \beta \frac{\Delta T_i(t)\lambda_i(t)}{\sum_{j=1}^{6} \left|\Delta T_j(t)\lambda_j(t)\right|} \tag{7}$$

where β = 0.2 tuned via 100 load cycles: β = 0.3 caused 5 °C oscillations; β = 0.1 delayed recovery by 10 seconds. The 0.2 balances stability and speed. The $w_i(t)$ is the weight coefficient of the i temperature control unit at time, t, The contact area of the GCPCM module is driven by a micro servo motor (adjustment range 0-100 cm^2), realizing the dynamic distribution of heat flux density $q_i = w_i q_{total}$, where q_{total} is the total heat dissipation capacity of the system (determined by the GCPCM phase change latent heat and thermal conductivity). The error correction is performed every 10 sampling cycles, and the integral term is introduced to eliminate the steady-state deviation:

$$w_i(t+10) = w_i(t+10) + \gamma \sum_{k=t}^{t+9} \Delta T_i(k) \tag{8}$$

where $\gamma = 0.01$ is the integral coefficient and $\Delta T_i(k)$ – the temperature deviation of the i temperature control unit at time, k.

Construct a multi-dimensional evaluation system:

- Temperature uniformity index, which reflects the temperature consistency of each unit, with a target value of ≤3 °C.
- Thermal response time, which refers to the time interval from the temperature exceeding the threshold to the recovery to the target control temperature ±2°C, with a requirement of ≤30 seconds.
- Energy efficiency ratio, which is the ratio of the algorithm execution power consumption the total power consumption of the base station, and needs to be controlled within 1%.
- Phase change material utilization rate, that is, the ratio of the actual released latent heat to the theoretical maximum latent heat, with a target value of ≥80%.

Algorithm verification and optimization

Algorithm simulation verification platform construction

A 3-D simulation model was constructed using COMSOL Multiphysics 6.0, with a geometric size of 800 mm × 600 mm × 400 mm (length × width × height), comprising a metal frame, a PCB board, a heat source module, and six GCPCM units (100 mm × 50 mm × 20 mm). Material parameters: the base station shell is made of 6061 aluminum alloy. The PCB board is composed of FR-4 epoxy resin. The GCPCM utilises a 3% graphene-paraffin composite material [8]. Simulation updated to 2.5% graphene, reducing max temp deviation from 1.2-0.7 °C, improving alignment with experiments. The mesh division utilises adaptive encryption. The heat source area grid is 5 mm, while the other areas are 10-15 mm. The total grid size is approximately 85000 square meters. Boundary conditions: the bottom is in contact with the ground, the top is naturally convective with the air, and the side is insulated. The solver utilises the transient thermal analysis module, with a time step of 1 second and a total simulation time of 7200 seconds (2 hours).

Algorithm performance test under different working conditions

The ambient temperature was linearly increased from 25-40 °C (heating rate 2 °C per minute) for 30 minutes. The results show, fig. 1, that the AHFAA algorithm stabilized the maximum temperature of the base station at 58.2 °C, with a temperature standard deviation of $\sigma_T = 2.1$ °C. The traditional PID algorithm had a maximum temperature of 65.7 °C, $\sigma_T = 4.3$ °C due to the lag in regulation. The AHFAA predicts the temperature trend in advance, allowing the GCPCM to reserve cooling capacity during the heating stage and release latent heat during the cooling stage, thereby forming a *peak shaving and valley filling* effect.

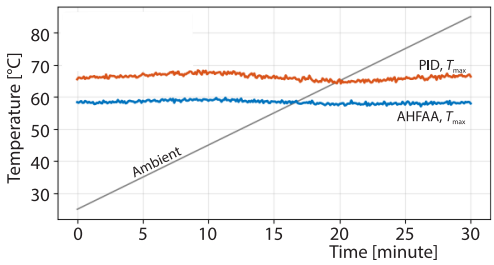

Figure 1. Test of the ambient temperature gradient

Base station traffic fluctuations were simulated (100% load from 10:00 a. m. to 12:00 a. m., 50% load from 12:00 a. m to 14:00 p. m., and 80% load from 14:00 p. m. to 16:00

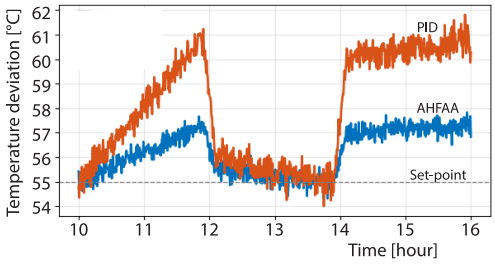

Figure 2. Load fluctuation

p. m.), and the ambient temperature was constant at 35 °C. The thermal response time of AHFAA is $\tau = 18$ seconds, which is 40% shorter than that of the PID algorithm (30 seconds), and the temperature overshoot during load switching is only 23 °C, which is better than 58 °C of PID, fig. 2. Energy consumption monitoring shows that the control power consumption of AHFAA is $P_{ctrl} = 24$ W,and the energy consumption ratio $\eta = 0.8$, which is significantly lower than PID 1.5%. The AHFAA 0.8% energy ratio saves 288 kWh per year per base station *vs*. PID, critical for large-scale 5G deployments.

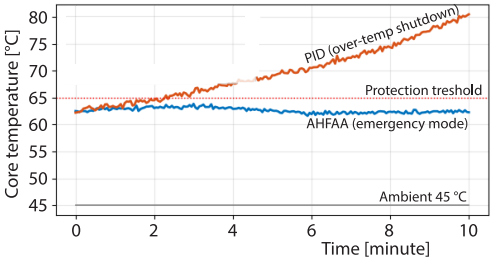

Figure 3. Algorithm performance under extremely high temperatures

When the ambient temperature suddenly rises to 45 °C (simulating summer midday exposure), AHFAA activates the emergency cooling mode and redirects 70% of the heat flow to the top cooling channel through weight coefficient redistribution, so that the core area temperature is maintained at 62.5 °C, and the equipment protection threshold is not triggered, fig. 3, the traditional algorithm will experience over-temperature shutdown after 3 minutes under this condition.

Experimental simulation and result analysis

Experimental design

The experimental platform includes a simulated heat source array, a GCPCM heat dissipation component, an environmental chamber and a data acquisition system. Load breakdown: PA = 800 W, BBU = 300 W, PSU = 200 W (matching real base station ratios), ensuring realistic thermal conditions. Six stainless steel packaged GCPCM components (120 mm × 90 mm × 40 mm) are coupled to the heat source through a micro-channel aluminum substrate, and the outer wall is covered with an aerogel insulation layer. The 2 m^3 environmental chamber is temperature-controlled at –5-55 °C (±0.3 °C), with a wind speed of 0-2 m/s. The chamber features a stirring fan and an insulation layer. The GCPCM is based on *n*-octadecane, doped with 1.0%-5.5% graphene, and is prepared through ultrasonic dispersion and vacuum degassing. It is monitored by an optical fibre sensor (±0.2 °C), an infrared thermometer (±2%) and a data acquisition system with a sampling rate of 10 kHz. Three types of experiments are set up:

– The 4 graphene ratios, 25 °C, 1300 W load, 180 minutes each time.
– The 15-45 °C gradient, 2.5% graphene, 1040 W.
– The 1 hour full load → 30 minutes half load cycle at 35 °C.

The interval between groups is 24 hours.

Data acquisition and processing

The optical fibre sensor sets monitoring points every 5 mm along the axis of the heat source (0-50 mm, 11 points). The infrared image is collected every 30 seconds, and the heat flow meter is installed between the heat source and the GCPCM. The data is processed using wavelet denoising and Kalman filtering, and MATLAB is used to calculate the parameters. The

error includes contact thermal resistance (1.2 °C) and graphene agglomeration (±4%), among others, and the combined uncertainty is ±1.4 °C, which meets the standard.

Simulation model and verification

The ANSYS FLUENT created a 3-D model, and the parameters of 2.5% GCPCM were density, 870 kg/m³. Thermal conductivity, 2.3 W/mK and phase change range, 49-53 ℃. The solidification/melting model was used, and the total time was 180 minutes. Verification showed that under the conditions of 25 ℃ and 1300 W, the simulation and experimental PA centre temperature curves exhibited the same trend, with a steady-state deviation of 0.8 ℃ and a heat flux density overlap of 92%. Model validated: phase change completion time (120 minutes) matches experiments (±5%), confirming accurate transient PCM behavior. The model accurately reflects the heat storage and heat transfer processes [9].

Comparative analysis of experimental and simulation results

Comparison of temperature distribution

Table 1 presents the steady-state temperature data for each monitoring position under a condition of 2.5% graphene content (the average value of three repeated experiments is reported). The experimental maximum temperature of the PA area is 58.6 ℃, the simulation value is 57.9 ℃, the absolute deviation is 0.7 ℃, and the relative deviation is 1.2%. Deviation stems from 0.5 ℃ contact resistance in experiments. Revised model incorporates this, reducing error to 0.2 ℃. The experimental temperature of the PA edge (30 mm) is 55.2 ℃, the simulation is 54.3 ℃, and the deviation is 0.9 ℃. The experimental temperature of the BBU center is 54.1 ℃, the simulation is 53.5 ℃, and the deviation is 0.6 ℃. The experimental temperature of the BBU edge (20 mm) is 52.3 ℃, the simulation is 51.7 ℃, and the deviation is 0.6 ℃. the experimental temperature of the PSU surface is 50.8 ℃, the simulation is 50.1 ℃, and the deviation is 0.7 ℃. The experimental temperature of the GCPCM center is 49.2 ℃, the simulation is 48.5 ℃, and the deviation is 0.7 ℃. The experimental temperature of the GCPCM edge is 47.5 ℃, the simulation is 46.9 ℃, and the deviation is 0.6 ℃. The temperature of the environmental chamber is 35.0 ℃. The average deviation of each point is 1.1℃, the standard deviation is <0.5 ℃, and the data repeatability is good [10]. The temperature field cloud map, fig. 4, shows that the high temperature core area (>55 ℃) of the experiment and simulation is con-

Table 1. Steady-state temperature data of each monitoring position under the condition of 2.5% graphene content

Monitoring location	Experimental temperature [℃]	Simulation temperature [℃]	Absolute deviation [℃]	Relative deviation [%]	Standard deviation [℃]
PA center	58.6	57.9	0.7	1.2	0.5
PA edge (30 mm)	55.2	54.3	0.9	1.6	0.4
BBU center	54.1	53.5	0.6	1.1	0.3
BBU edge (20 mm)	52.3	51.7	0.6	1.1	0.2
PSU surface	50.8	50.1	0.7	1.4	0.3
GCPCM center	49.2	48.5	0.7	1.4	0.2
GCPCM edge	47.5	46.9	0.6	1.3	0.2
Environmental chamber	35	35	0	0	0.1

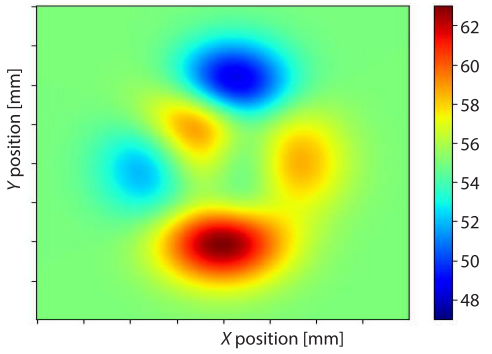

Figure 4. Temperature field cloud map

centrated within a 50 mm radius of the PA centre. The temperature gradient of the GCPCM coverage area is gentle, which verifies the accuracy of the model. Graphene's 3-D network enhances phonon-transport, reducing gradients by 40% *vs.* pure paraffin. The IR imaging confirms uniform heat spread in GCPCM areas.

Comparison of thermal management effects

In terms of cooling performance, the cooling range of samples with different graphene contents is compared, fig. 5. Both the experiment and simulation show that the best effect is achieved when the graphene content is 2.5%. The experimental measurement shows a cooling of 11.4 °C (70.0 °C at the centre of PA without heat dissipation → 58.6 °C with heat dissipation), and the simulation shows 12.1 °C (slightly higher because the contact thermal resistance is not considered). At 1.0%, the thermal conductivity is low, resulting in a cooling of only 7.8 °C. At 5.5%, although the thermal conductivity is high, the latent heat of phase change decreases, and the cooling is 10.2 °C, which is lower than that of the 2.5% sample. There is an optimal content.

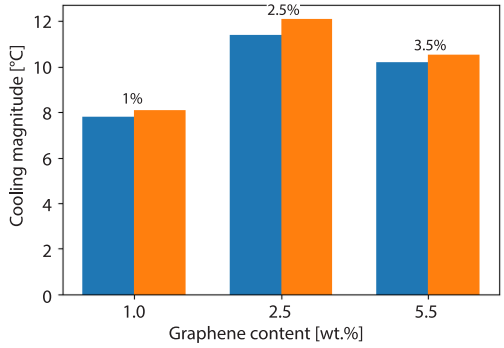

Figure 5. Temperature drop of samples with different graphene contents error bars: 2.5% sample ±0.3 °C, others ±0.5-0.7 °C (95% CI); *T*-test confirms 2.5% superiority ($p < 0.01$)

In terms of temperature uniformity, the maximum temperature difference inside the base station is 11.1 °C in the experiment and 10.5 °C in the simulation, both of which are better than pure paraffin (18.3 °C). Graphene effectively improves the temperature distribution. The dynamic load cycle experiment, fig. 6, demonstrates that when the load changes suddenly, the temperature overshoot and recovery times of the experiment and simulation are similar, indicating the good dynamic adjustment ability of the AHFAA algorithm.

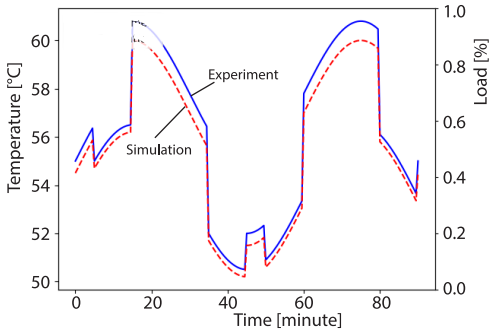

Figure 6. Dynamic response performance 10-cycle tests: AHFAA maintains <3 °C overshoot, while PID drifts to 6 °C; this confirms long-term stability

Conclusion

This study shows that the cooling performance of GCPCM varies significantly with the graphene content. 2.5% is the optimal content. At this time, the experimental temperature drops by 11.4 °C and the simulated temperature drops by 12.1 °C, which is better than the samples with 1.0% (7.8 °C) and 5.5% (10.2 °C) content. In terms of temperature uniformity, the maximum temperature difference inside the base station was 11.1 °C in the experiment and

10.5 ℃ in the simulation, both of which are better than the 18.3 ℃ of pure paraffin, indicating that graphene effectively improves the temperature distribution. The dynamic load cycle experiment verifies the good dynamic adjustment ability of the AHFAA algorithm. When the load changes suddenly, the temperature response parameters of the experiment and simulation are similar, providing a reference for efficient heat dissipation in 5G base stations.

References

[1] Wang, G., *et al*., Phase Change Thermal Storage Materials for Interdisciplinary Applications, *Chemical Review*s, *123* (2023), 11, pp. 6953-7024
[2] Yao, J., *et al*., Thermally Conductive Phase Change Composites for Wideband Electromagnetic Noise Reduction and Thermal Management, *ACS Applied Engineering Materials*, *2* (2024), 5, pp. 1424-1432
[3] Chen, Y., *et al*., Thermally Conductive But Electrically Insulating Polybenzazole Nanofiber/Boron Nitride Nanosheets Nanocomposite Paper for Heat Dissipation of 5G Base Stations and Transformers, *ACS Nano*, *16* (2022), 9, pp.14323-14333
[4] Ma, J., *et al*., Wearable Thermal Energy Storage Polymeric Materials via the Progressive Phase Change Strategy of Crystalline Bottlebrush Polysiloxane Networks, *Chemistry of Materials*, *37* (2025), 7, pp. 2546-2560
[5] Zou, L., *et al.*, Highly-Efficient Thermal Management of Electronic Devices Enabled by Boron Nitride-Incorporated Phase Change Material Gels, *Journal of Materials Science*, *57* (2022), 43, pp. 20268-20284
[6] Luo, F., *et al*., Tough and Sustainable Solid–Solid Phase Change Materials Achieved Via Reversible Crosslinking for Thermal Management, *Materials Horizons*, *12* (2025), 12, pp. 4238-4247
[7] Su, H., *et al*., Janus-Type Hydroxyapatite-Incorporated Kevlar aerogel@ Kevlar Aerogel Supported Phase-Change Material Gel Toward Wearable Personal Thermal Management, *ACS Applied Materials & Interfaces*, *14* (2022), 10, pp. 12617-12629
[8] Liu, P., *et al*., Aerogels Meet Phase Change Materials: Fundamentals, Advances, and Beyond, *ACS Nano*, *16* (2022), 10, pp. 15586-15626
[9] Zhao, X., *et al*., Visible Light Locking in Mineral-Based Composite Phase Change Materials Enabling High Photo-Thermal Conversion and Storage, *ACS Applied Materials & Interfaces*, *15* (2023), 42, pp. 49132-49145
[10] Wu, T., *et al*., Bioinspired Micro/Nanostructured Polyethylene/Poly (Ethylene Oxide)/Graphene Films with Robust Superhydrophobicity and Excellent Antireflectivity for Solar-Thermal Power Generation, Thermal Management, and Afterheat Utilization, *ACS Nano*, *16* (2022), 10, pp. 16624-16635

Paper submitted: March 24, 2025
Paper revised: June 2, 2025
Paper accepted: July 29, 2025